Characterization and interpretation of strongly nonlinear phenomena in fusion, space and astrophysical plasmas

2006 Plasma Phys. Control. Fusion 48 B313

(http://iopscience.iop.org/0741-3335/48/12B/S30)

INSTITUTE OF PHYSICS PUBLISHING PLASMA PHYSICS AND CONTROLLED FUSION

Plasma Phys. Control. Fusion **48** (2006) B313–B328 doi:10.1088/0741-3335/48/12B/S30

Characterization and interpretation of strongly nonlinear phenomena in fusion, space and astrophysical plasmas

R O Dendy[1,2] **and S C Chapman**[2]

[1] Euratom/UKAEA Fusion Association, Culham Science Centre, Abingdon, Oxfordshire, OX14 3DB, UK
[2] Centre for Fusion, Space and Astrophysics, Department of Physics, Warwick University, Coventry, CV4 7AL, UK

Received 23 June 2006
Published 13 November 2006
Online at stacks.iop.org/PPCF/48/B313

Abstract

Much of plasma behaviour is governed by multiple distinct nonlinear processes, operating on a wide range of lengthscales and timescales, that are coupled together in innumerable feedback loops. Capturing and quantifying this nonlinear behaviour is crucial at all levels of description, ranging from individual events to global phenomenology. In recent years, a range of techniques derived from complex systems science has been applied successfully to nonlinear plasma datasets. The present paper reviews several of these techniques in the context of applications spanning fusion, space, solar and astrophysical plasmas. Topics include non-Gaussian probability density functions, notably extreme event distributions in fusion and astrophysics and power law distributions in the solar context; differencing and rescaling of fluctuation data, which has yielded information on the number of dominant plasma turbulent processes, and the spatiotemporal ranges over which they operate, in plasmas ranging from microquasar accretion discs to L-mode and dithering H-mode fusion plasmas in the MAST tokamak; quantitative measures of mutual information content and pattern repetition between causally linked but spatiotemporally separated nonlinear events in solar wind and magnetospheric plasmas; global statistics of full-disc solar irradiance; and ELMing, considered as a sequence of pulsed events, in H-mode fusion plasmas in the JET tokamak. These developments in nonlinear plasma data characterization provide fresh additional insights into the underlying plasma physics. They also provide new opportunities for comparing models with data, and with each other, and open avenues for the development of a more rigorous predictive capability in this field.

(Some figures in this article are in colour only in the electronic version)

1. Introduction

During the past decade, there have been impressive advances in the quality of diagnostic information obtained from magnetically confined fusion plasmas. Similar qualitative advances have taken place in the observation of naturally occurring high temperature plasmas, notably in space physics, solar physics and x-ray astronomy. The temporal and spatial resolution of plasma diagnostic measurements and observations, together with the volume of data available for analysis, have progressed by orders of magnitude. In both natural and fusion plasmas, much of this data relates to phenomena that are strongly nonlinear or turbulent, and furthermore these nonlinear phenomena are central to the behaviour or performance of the plasma systems observed. These high-resolution, large volume nonlinear datasets repay systematic quantitative analysis using the new techniques outlined in this review. In particular, generic techniques are required, that can capture and quantify the essentially nonlinear features of the phenomenology. Fortunately, such techniques have been developed elsewhere in physics [1–3] during the past dozen years. These new nonlinear techniques complement Fourier-derived methods such as the power spectrum and autocorrelation [4], which are essentially linear and are not oriented towards capturing and quantifying nonlinear phenomenology. Of course, the conventional linear techniques retain value even in strongly nonlinear regimes, however some key physics can elude them.

Equally impressive have been the recent advances in plasma modelling, exploiting progress in computational physics; see, for example, [5] in the fusion context. The ingredients included in any particular model of a given plasma system necessarily reflect the selection criteria of the model's designers. While these criteria embody, so far as possible, the best understanding of the plasma physics involved, they are also constrained by considerations such as analytical tractability or computational resources. This raises fundamental questions. What, precisely, constitutes agreement between the output of a given nonlinear model and the observations of the corresponding nonlinear plasma system? Upon what basis can one model be said to agree better than another with the observed data? To what extent can one quantify the predictive capability of such models? A necessary condition for progress is to apply quantitative methods that extract model-independent information from the observed nonlinear signals from the real plasmas.

In the present paper, which is intended to have a partly tutorial flavour and for this reason is oriented towards our own research, we focus on the quantitative characterization of strongly nonlinear plasma phenomenology in a broad range of specific instances. These span magnetic confinement fusion—edge turbulence in the MAST spherical tokamak [6] measured by probe saturation currents, and ELMing in JET H-mode plasmas [7]; astrophysical x-ray sources—the microquasar GRS 1915+105 and the black hole x-ray binary Cygnus X-1 [8, 9], measured by the All-Sky Monitor onboard the RXTE satellite; the solar corona—fluctuations in the full-disc extreme ultraviolet/soft x-ray irradiance [10], measured using the CELIAS/SEM instrument onboard the SOHO spacecraft; and the causal linkage [11, 12] between nonlinear fluctuations in the far upstream solar wind, measured by the WIND satellite at the sunward libration point and currents in the auroral zone of the terrestrial magnetosphere, measured by a magnetometer chain at high geomagnetic latitude. Figure 1 shows six examples of measured time series of strongly nonlinear plasma phenomenology drawn from fusion, astrophysics and solar contexts. These demonstrate the generic nature of the plasma physics challenge we have outlined. To help focus on this, in figure 1 we have suppressed the axis labels: the intensities relate to various forms of photon count or current amplitude and the durations of the time series range from tens of milliseconds (MAST edge turbulence) to five years (GRS1915 + 105 x-ray signal). We refer to the original papers for specifics.

Before turning to these practical examples, it may be helpful to make three further remarks. First, the investigations reviewed here are essentially pilot studies. They demonstrate that the

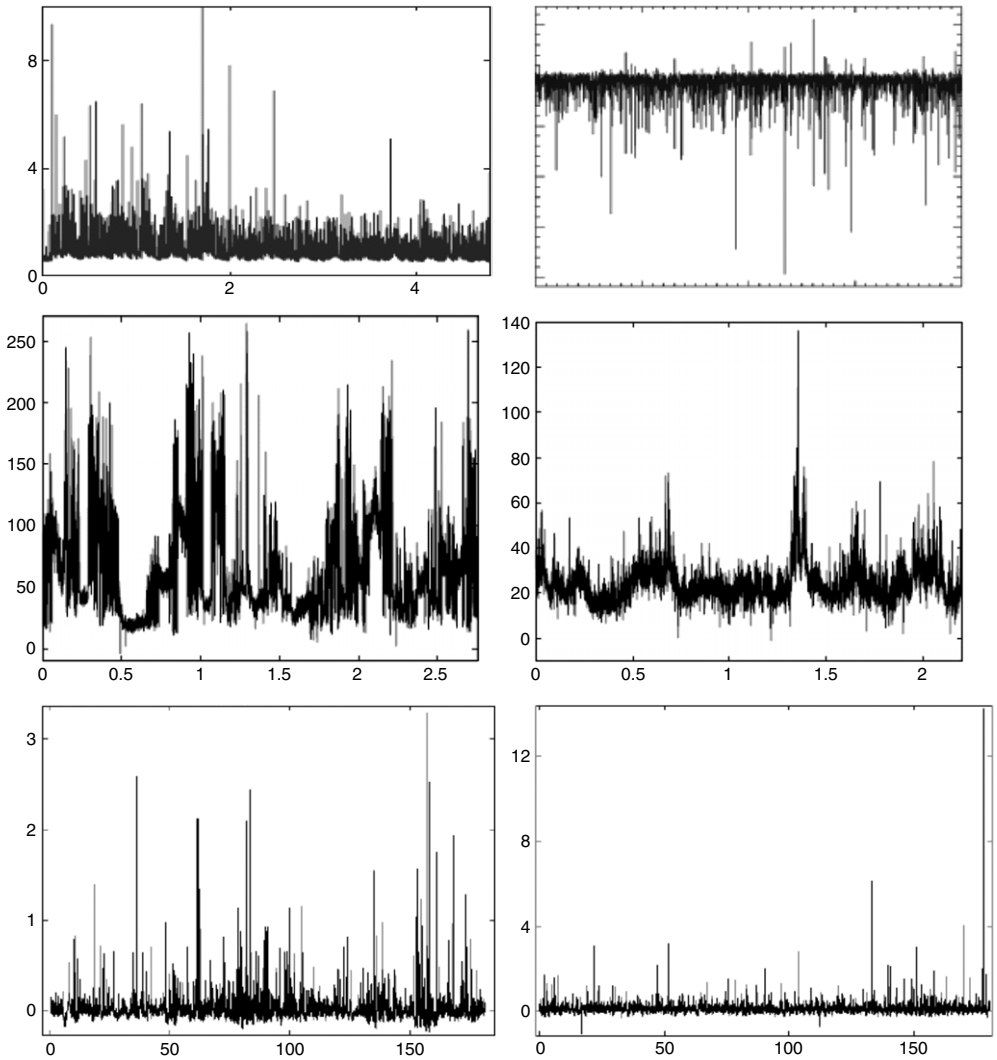

Figure 1. The generic nature of strongly nonlinear plasma phenomenology is illustrated by measured time series spanning fusion, astrophysics and solar physics. Top pair: (left) Type III ELMing [7] over 4 s in JET H-mode plasma 43992; (right) edge turbulence [6] from the ion saturation current measured in an edge probe over 40 ms in MAST L-mode plasma 6861. Middle pair: x-ray intensities [8] from (left) the microquasar GRS 1915+105 observed over five years 1996–2001 and (right) the x-ray binary Cygnus X-1 observed over three years 1996–1999. Bottom pair: detrended full disc EUV/XUV solar irradiance [10] over six months during periods of high (left—year 2000) and low (right—year 1996) solar activity.

new generic techniques for characterizing strongly nonlinear datasets do actually work and yield physically useful information, for macroscopic plasmas. There is no particular *a priori* reason to expect this success: the techniques were developed primarily for application to quasistationary tabletop nonlinear systems, whereas macroscopic plasma phenomenology typically extends over a very wide range of lengthscales and timescales. This brings us to our second remark that, because of their wide range of operative scales and their very large number of degrees of freedom, macroscopic plasmas fall within the ambit of contemporary complex

systems science. There are two main themes to this emerging field, both of which are relevant to plasma physics. In addition to the development of the techniques for capturing and quantifying nonlinearity, whose plasma applications are reviewed below, there is the construction of minimalist models [13–23] believed to embody the key physics of a given system, and the examination of how far such models display global nonlinear phenomenology and statistics similar to those of the real system. For a topical review of this aspect of complex systems science applied to fusion, space and solar plasmas, we refer to [23]. Third, we remark that the quantitative results reviewed below are, importantly, model-independent. By this we mean that the numbers that emerge from the analysis are direct properties of the data, as distinct from numbers that assume a particular model, such as diffusivities inferred from fitting energy transport data to a diffusion equation. It follows that these results provide an impartial measure against which different models can in future be compared. Insofar as these techniques, applied to the output of a given model—for example, a large scale numerical simulation embodying a particular set of reduced equations—yield numbers close to those obtained from application to the real data, the model in question is quantitatively successful in capturing the essential nonlinear phenomenology of the real system. These pilot studies thus provide the foundation for a substantial step forward in the development of a rigorous modelling, interpretive and predictive capability for nonlinear and turbulent phenomena in high temperature plasmas of all kinds.

2. Non-Gaussian probability density functions for astrophysical and fusion plasma datasets

The concept of a measured magnitude-frequency plot which, suitably normalized, becomes a probability density function (PDF) requires no introduction. Less familiar, but relevant in the present context, is the extent to which contemporary statistical physics provides a basis for understanding families of PDFs that are strongly non-Gaussian, in particular that are long-tailed through having significantly more large events. Extreme event distributions [3], for example, can be used to fit the PDFs of x-ray signal intensities [8] emitted from the astrophysical accretion disc plasmas in the microquasar GRS 1915 + 105 and the black hole x-ray binary Cygnus X-1 (raw data is displayed in the middle panels of figure 1) and also the PDFs of ion saturation current measurements of edge turbulence [6] in the MAST spherical tokamak (for an example of the raw data see the top right panel of figure 1); see figures 2 and 3, respectively. Such distributions result from repeatedly selecting the maximum value from each of a large number of large samples—the brightest among many contemporaneous local flashes scattered across an extended object, for example. Physically, the fact that the tails of the PDFs in figure 2 can be fitted by extreme value distributions suggests that the observed signals may be maximal events in this sense—they are the brightest among multiple events occurring within each time window.

3. Statistics of pulsed phenomena in plasmas

The occurrence of well-defined nonlinear events, highly structured in space and time—as distinct from the turbulent fluctuations considered in the preceding section—is widespread in fusion and natural plasmas. A classic study in plasma event statistics concerns the measured magnitude–frequency plot of the brightest solar x-ray flares. This is found [24, 25] to have power law slope extending over several decades in event magnitude, and independent of the phase of the solar cycle, thus providing observational motivation for the conjecture [22,26] that the solar coronal plasma and magnetic field may be in a state of self-organized criticality [13]. In magnetically confined fusion plasmas, edge localized modes (ELMs; see the top left panel of figure 1), whose characteristics are deeply linked to the overall confinement properties

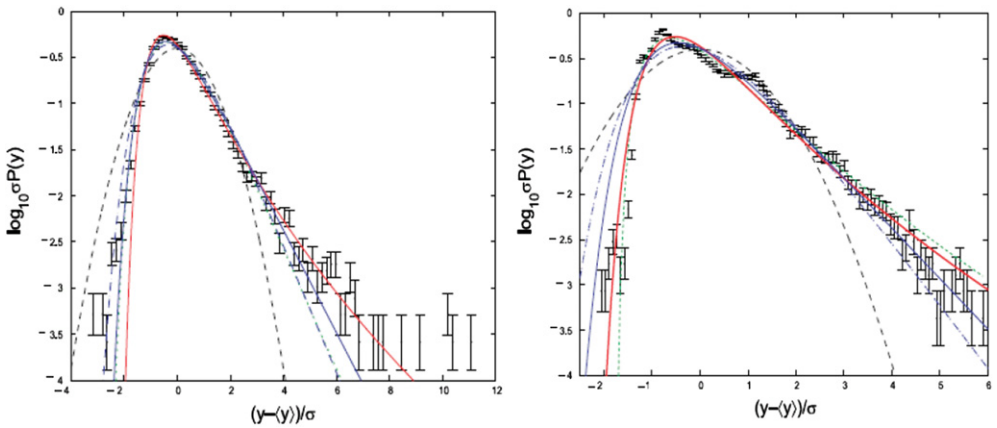

Figure 2. Long-tailed PDFs of the x-ray signal intensity [8] observed from (left) Cygnus X-1 and (right) GRS 1915 + 105 accretion disc plasmas, showing strong deviation from the Gaussian (dashed black lines). The coloured curves represent best fits of different classes of known extreme value distribution functions to these long-tailed datasets.

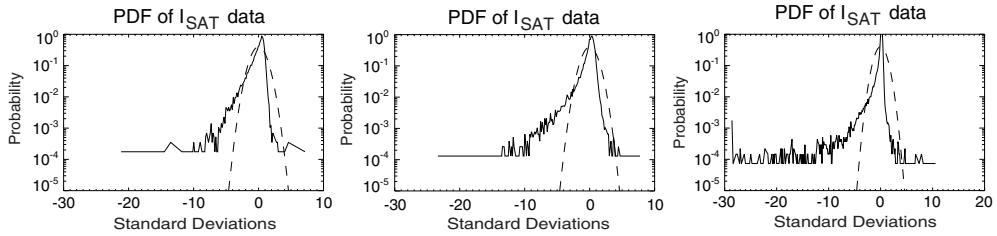

Figure 3. Long-tailed PDFs of the ion saturation current [6] measured from a probe in the turbulent MAST edge plasma under different confinement regimes. L-mode plasma 6861 (left); dithering H-mode plasma 9031 (centre); H-mode plasma 5738 (right). Dashed lines define the Gaussian.

of the plasma, provide a well-defined dataset of pulsed events. The statistical properties of measured ELM sequences [7, 27, 28] should provide a rich field of research, shedding fresh quantitative light on plasma confinement. However, ELM measurements are challenging insofar as magnetically confined fusion plasmas are seldom quasistationary on timescales long enough to enable robust ELM statistics to be constructed. Establishing the statistical character of different ELMing processes would nevertheless provide important model-independent quantitative descriptors of the data, while also constraining models of this strongly nonlinear phenomenon. Given an ELM sequence, one may ask to what extent does this reflect a statistical process which is quasiperiodic or, on the contrary, random?

A pilot study of the statistics of ELMs, previously identified as Type III, is reported in [7] for four similar JET plasmas which differed in isotopic concentration. Despite the challenging nature of the datasets, from this statistical perspective surprisingly robust conclusions can be drawn, which differentiate significantly between the Type III ELMing processes in the different plasmas. Inverse exponential PDFs of the time intervals between Type III ELMs are found for two of these four JET plasmas (44028 and 43392, whose raw signal is displayed in the top left panel of figure 1), with goodness-of-fit parameter $R^2 = 0.96$ and 0.93, respectively, as distinct from the Gaussian distribution expected for a quasiperiodic process [7]. See, for example, figure 4. Inverse exponential PDFs for the intervals between events arise naturally from Poisson processes. This suggests that the ELMs in JET plasmas 43392 and 44028 might

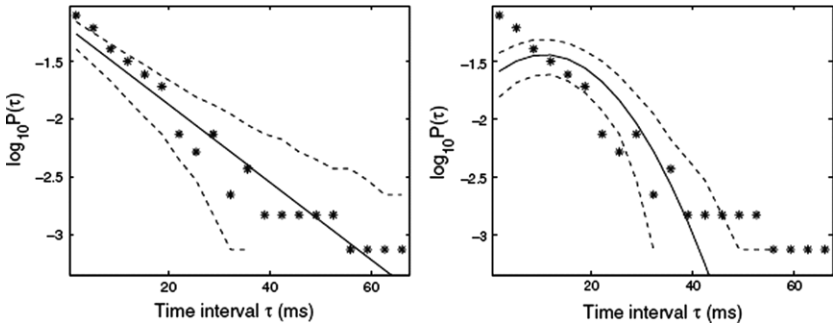

Figure 4. PDFs of time intervals τ between ELM events for JET plasma 43392, showing two attempted functional fits [7]. Inverse exponential fitted by least squares, for which the goodness-of-fit parameter $R^2 = 0.96$ (left). Gaussian model with the same μ and σ as the data, for which $R^2 = 0.31$ (right). Dashed lines indicate upper and lower confidence limits inferred from 99% binomial counting errors.

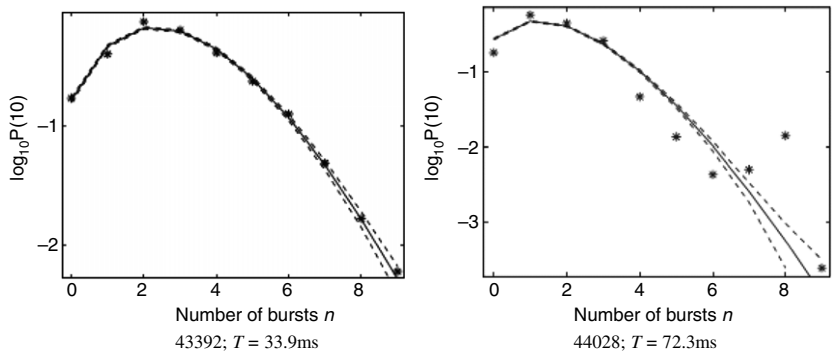

Figure 5. Testing the Poisson hypothesis [7] for the ELMing process in two similar JET plasmas: PDFs for the number n of ELM events occurring within time interval T. ——: Poisson distributions having the same μ as the data. - - - -: 99% binomial counting errors. Computed goodness-of-fit parameter $R^2 = 0.72$ (43392, left) and 0.15 (44028, right).

arise from a Poisson process, for which there is a constant probability per unit time of an event occurring (the antithesis of quasiperiodicity), and the number of bursts occurring in an arbitrary fixed time interval is Poisson distributed. To test this hypothesis, figure 5 plots the PDFs for the number n of ELM bursts occurring within a fixed time interval T, in these two JET plasmas [7]. The value of T is chosen to be sufficiently large for a range of values of n to be observed but not so large that a Poisson distribution will approach its Gaussian high-mean limit (a Gaussian PDF would be parabolic on these plots). The solid lines are Poisson PDFs that have the same mean μ as the data, and the closely adjacent dashed lines are for 99% binomial counting errors. It is clear from figure 5 that only the distribution of bursts in JET plasma 43392 is consistent with a Poisson process. Its value of R^2 is 0.72 compared with 0.15 for JET plasma 44028.

These simple model-independent statistical analyses [7] of the ELM datasets partition them neatly: first, into pairs, according to the functional form of the PDFs of inter-ELM time intervals; second, within one of these pairs, into a Poisson and a non-Poisson process. This provides a rigorous quantitative basis for ELM classification, while strongly suggesting that there is considerable diversity within the Type III category. It implies that there remains much to be learnt about the fundamental physics of the ELMing process, while providing a focus

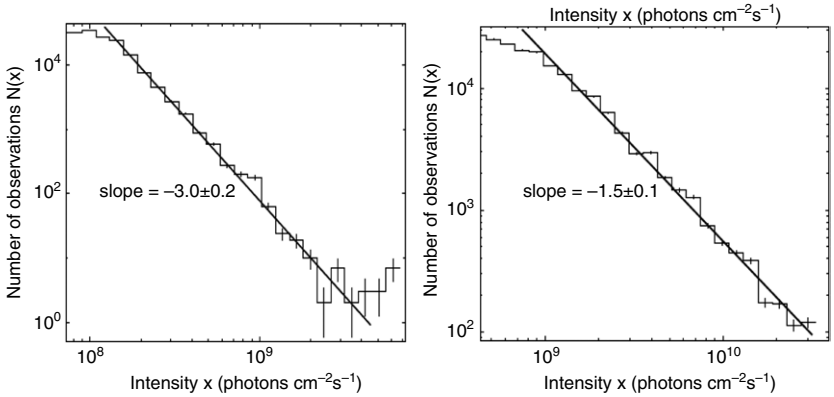

Figure 6. Log–log tails of distributions of full-disc solar EUV/XUV flux [10], observed at 15 s intervals by SOHO/SEM. During low solar activity, 1996 January–June (left). During high solar activity, 2000 January–June (right). Slopes are calculated using least-squares, with 95% confidence levels. Vertical error bars indicate a factor of $\pm N^{-1/2}$, bin widths indicate horizontal errors.

(in particular, as regards the Poisson process) for further quantitative investigation, and also constraining ELM models.

4. Statistics of globally integrated solar coronal plasma behaviour

The study of event statistics in plasma physics relies on criteria for identifying events. These criteria may sometimes be unambiguous, as for strong ELMs, but may sometimes incorporate an element of subjectivity, and therefore incompleteness. When does a fluctuation become an event? Early studies of event statistics in magnetospheric plasma physics, for example the pioneering work of Consolini [29], defined an event as occurring whenever the observed signal amplitude exceeded a certain threshold. The active solar coronal plasma and magnetic field can, from one perspective, be considered as comprising the superposition of multiple impulsive events, occurring on many different lengthscales and timescales. These range from the largest flares (10^{33} ergs) down to nanoflares (10^{24} ergs) and possibly beyond. In principle, all these events are distinguishable, and indeed the statistics of large flares was the subject of important early studies, as noted previously. In practice, however, not all flare activity can be identified by event selection from images. Furthermore there are important radiative, but nonflaring, contributions to the solar coronal energy budget: these include waves, slow flows and coronal mass ejections. This example illustrates a general point: there are benefits, particularly from a model-independent perspective, in studying globally integrated statistics, which do not rest on the specific criteria needed to define events, nor on the observational capability to capture a proper sample of all such events.

Here we consider a practical example of global statistics in plasma physics and show that useful quantitative information and physical insights emerge. The bottom pair of panels in figure 1 shows the measured EUV/XUV irradiance of the Sun [10], integrated across the full solar disc and averaged over 15 s intervals, for periods of six months. These datasets thus sum over all the various physical processes outlined in the preceding paragraph. The datasets have been detrended, so as to remove the consequences of the motion of active regions across the solar disc with the Sun's 27-day rotation period. Detrending is achieved by subtracting from each data point the mean of the measurements over a 40-h period (10^4 15 s sampling intervals) centred on that point. This period is chosen to be much less than the timescale to be removed (27 days) and much greater than the timescales of interest. Figure 6 shows the

measured PDFs [10] of the higher-energy tails of these datasets at times of low and high solar activity. In both cases, a well-defined exponent emerges from this exercise, with goodness-of-fit parameter $R^2 = 0.99$. The values of the exponent are integer and half-integer and differ by a factor of two between periods of low and high solar activity. We have thus obtained a robust model-independent quantifier of the integrated radiative properties of the full-disc solar coronal plasma and magnetic field, possessing mysteriously neat numerical values and differing substantially between different regimes of solar activity [10]. As with our previous examples of model-independent data characterization, these empirically obtained numbers would constrain any model of the global coronal plasma and magnetic field. To our knowledge, there exists no first-principles mathematical model of this system—incorporating, for example, equations describing very large numbers of interacting magnetic loop structures on a wide range of lengthscales. A complex systems approach has however recently been proposed and implemented [22], whose statistics of energy release events yield an index -3, like figure 6 (left).

5. Scaling and correlation of nonlinear astrophysical and fusion plasma phenomena

Considered as sequences of tens of thousands of digits, the datasets represented visually in figure 1 repay investigation using contemporary techniques of nonlinear time series analysis [1–3]. These techniques are designed to capture and quantify distinctively nonlinear properties, and thus differ from Fourier-derived techniques (for example, autocorrelation functions) which are best adapted to datasets reflecting coherence and linear superposability. Nonlinear time series analysis techniques are particularly well adapted to datasets that exhibit self-similarity, in the broad sense that a segment of the data, suitably stretched, resembles the whole in its statistical properties and indeed visually. While self-similarity, like the non-Gaussianity described in section 2, is a strong indicator of highly-correlated processes such as turbulence, there are no compelling reasons to expect nonlinear time series analysis techniques to work well in the practical plasma contexts which we now explore. Nevertheless, as we now discuss, both natural and fusion plasmas provide fruitful fields of application, where these techniques quantify the underlying physical processes successfully, and provide new insights.

5.1. Growth of range

The difference between the maximum and minimum values of a data time series $y(t)$ during an interval Δt defines its range $R(\Delta t)$ for that interval. Let a window of width Δt be run through the entire dataset and the value of $R(\Delta t)$ be computed at each step. An ensemble-averaged value $\langle R(\Delta t)\rangle$ can then be calculated, and this operation can be repeated for windows of different size Δt. If the time series $y(t)$ is self-similar, the ensemble-averaged value of the range will scale with window size: $\langle R(\Delta t)\rangle = c\Delta t^{\mathrm{H}}$, where c and H are constants. This equation defines the Hurst exponent H which quantifies the self-similar growth of range.

Figure 7 displays the results of applying this procedure to three plasma datasets shown in figure 1. The astrophysical examples [8] at left and centre in figure 7 correspond to the central pair of traces in figure 1, and the fusion plasma example [6] at right in figure 7 corresponds to the trace at top right in figure 1. It follows that the underlying plasma physics gives rise to signals that are self-similar to a significant extent, implying turbulent processes with substantial correlation over long timescales. Furthermore, it is possible to characterize this self-similarity by means of the single well-defined model-independent quantity H. The value of H both discriminates observationally between datasets and constrains models of these systems: for example, a numerical simulation of MAST edge turbulence under the conditions of plasma

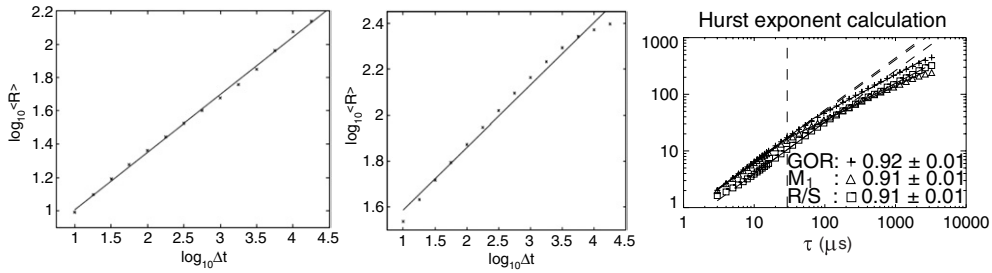

Figure 7. Growth of range. Logarithmic plots of $\langle R(\Delta t)\rangle$ versus Δt for x-ray time series from Cygnus X-1 (left) and GRS 1915 + 105 (centre) [8], where time steps are 90 min; and ion saturation current measurements in MAST L-mode plasma 6861 (right) [6], where time units are microseconds. The value of the Hurst exponent is well defined in all cases: 0.35 ± 0.1, 0.27 ± 0.2 and 0.91 ± 0.01, respectively.

6861 should generate a signal whose H-value matches that obtained in figure 7, and likewise for the astrophysical examples. The value of H for a given time series can be computed using a variety of algorithms, as in the right panel of figure 7.

5.2. Differencing and rescaling

Further information on the timescales over which nonlinear physical processes operate, and on their statistical character, together with confirmation of any correlation suggested by growth of range or autocorrelation studies, is clearly desirable. This can be provided by the differencing and rescaling technique, for which see [8] and references therein, as follows. The original data time series $y(t)$ can be used to construct a differenced time series $Z(t, \tau) = y(t) - y(t - \tau)$. This time series gives the sequence of fluctuations in the data, over a timescale τ, at each time step. Many values of τ can be chosen, each of which generates a differenced time series $Z(t, \tau)$ describing fluctuations on the corresponding timescale. Thus a family of differenced time series $Z(t, \tau)$ is generated from a single data time series $y(t)$. Fluctuation amplitudes Z are typically small when τ is small, because the dataset does not have time to diverge, whereas larger-amplitude fluctuations Z occur for larger τ, during which interval the dataset has time to diverge substantially. In general, the distribution of fluctuations within the dataset on timescale τ is described by the PDF $P(Z, \tau)$, known as the differenced distribution. For small τ, $P(Z, \tau)$ will typically be strongly peaked about $Z = 0$ and negligible for large Z, whereas $P(Z, \tau)$ will be significant at larger values of Z for larger τ.

If the fluctuations observed in the dataset are driven by a dominant underlying physical process which maintains correlation up to some timescale τ_c, and the fluctuations are self-similar, it follows that all members of the family of differenced distributions $P(Z, \tau\colon \tau < \tau_c)$ contain the same information. These distributions are, in essence, identical—they are simply stretched versions of each other. Mathematically, a simple rescaling operation applied to P and Z causes all the curves representing $P(Z, \tau)$ in this family to collapse onto a single curve, as follows. It will be found that the peak amplitudes $P(0, \tau)$ scale as $\tau^{-\alpha}$ for $\tau < \tau_c$, where the parameter α is inferred empirically. Rescaling $Z \to Z\tau^{-\alpha} = Z_s$ and $P \to P\tau^{\alpha} = P_s$ for each $P(Z, \tau)$ with $\tau < \tau_c$ creates rescaled PDFs which all collapse onto a single curve $P_s(Z_s)$ characteristic of the dominant physical process. To fix ideas, figure 8 shows differencing and rescaling in action for the simple example [8] of a Gaussian random walk $y(t)$.

If the procedure outlined above works for a given dataset, there emerge three new model-independent quantities characterizing the dominant physical process: the correlation timescale

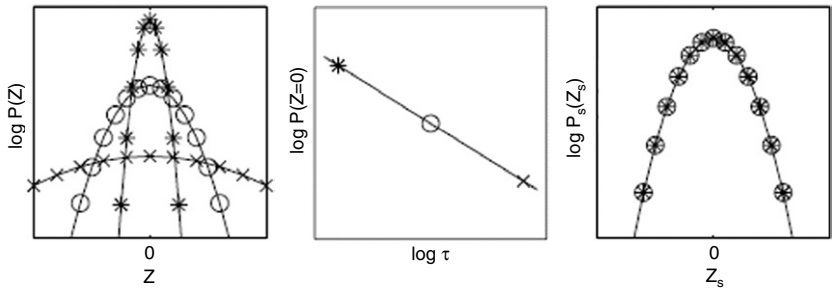

Figure 8. Rescaling differenced distributions $P(Z)$. Unscaled PDFs of differenced series constructed from a Gaussian random walk [8], showing curves for three different values of τ (left). Power law scaling of $P(0, \tau)$ with τ, whose slope yields the scaling parameter α (centre). Collapse of rescaled PDFs onto a single (Gaussian) curve for all τ (right).

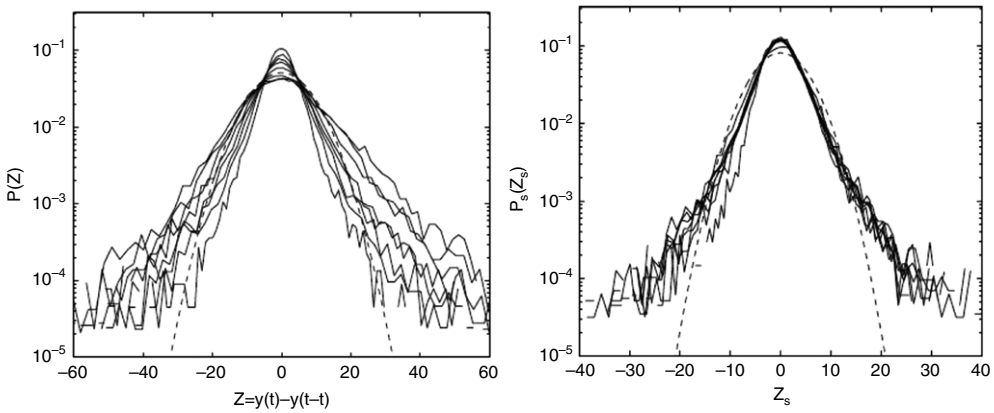

Figure 9. Unscaled PDFs $P(Z, \tau)$ of differenced time series of x-ray signals from Cygnus X-1, plotted versus Z, with differencing parameter τ stepping up in half-integer powers of the 90 min time step up to a maximum 10^4. Curves with lower $P(0)$ and broader tails correspond to higher values of τ. The scaling of $P(0)$ with τ yields the value of the parameter α used for rescaling (left). Rescaled PDFs $P_s(Z_s)$ plotted versus Z_s. The curves collapse onto a single characteristic distribution, which deviates substantially from a Gaussian (- - - -) (right) [8].

τ_c up to which the differencing and rescaling operation succeeds, and beyond which it breaks down; the scaling parameter α; and the shape of the curve onto which the differenced PDFs collapse. As with the growth of range analysis above, there are no compelling reasons to expect the differencing and rescaling technique to operate successfully in the plasma contexts of interest here. Nevertheless, it can do so: see, for example, figures 9 and 10. Physically, figure 9 establishes that the X-ray output of Cygnus X-1 is self-similar and correlated, with variations controlled by one type of non-Gaussian process, on timescales up to three years [8]. These model-independent results for the raw data displayed in the right central panel of figure 1 can be compared with those for the data from GRS 1915+105 in the left central panel of figure 1, for which differencing and rescaling operates successfully [8,9], but yields two well-defined rescaling regimes with different values for the scaling parameter α, with correlations on timescales of days. Figure 10 shows that this latter type of rescaling phenomenology is found [6] also for the MAST L-mode edge turbulence dataset shown in the top right panel of figure 1, with correlations on timescales of tens of microseconds.

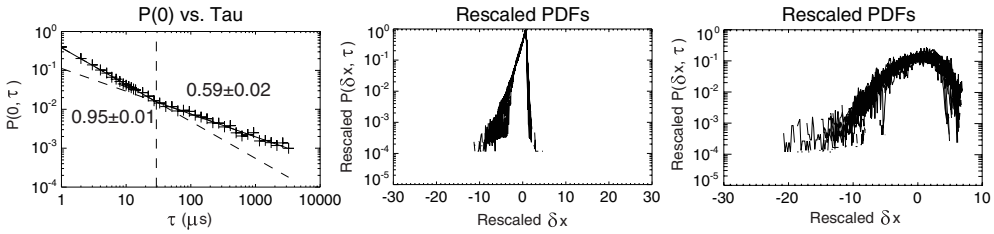

Figure 10. The value of $P(0, \tau)$ plotted versus τ for the family of differenced distributions $P(\delta x, \tau)$ constructed from ion saturation current (x) measurements in MAST L-mode plasma 6861. The scaling parameter α is well defined within two sharply separated regions (left). Collapse of rescaled PDFs for $\tau < 60\,\mu$s onto a single curve, using slope 0.95 from left panel (centre). Collapse of rescaled PDFs for $\tau > 60\,\mu$s onto a different single curve, using slope 0.59 from left panel [6] (right) .

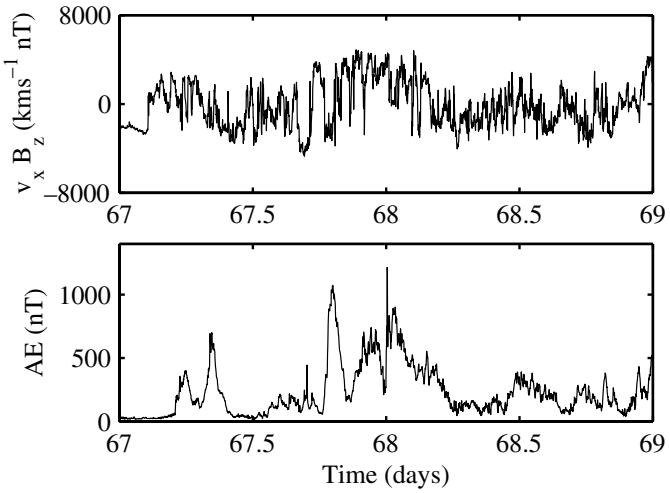

Figure 11. Solar wind fluctuations measured by the WIND satellite at the sunward libration point during the first half of 1995 (upper). Contemporaneous measurements of magnetic field fluctuations by a terrestrial magnetometer chain at high geomagnetic latitude (lower). From [11].

6. Information content of strongly nonlinear space plasma datasets

Information is a physical quantity, and the information content of strongly nonlinear signals from plasmas repays study insofar as it yields physical insights. As we describe in the following example, quantifying the mutual Shannon information [30] shared between two causally linked but spatiotemporally separated plasma signals [11,12] can identify key timescales; distinguish between plasma physics models for the propagation of perturbations; and measure the strength of the causal link. The upper trace of figure 11 displays measured fluctuations in the solar wind, far upstream of Earth, which subsequently propagate to the outer boundary layers of the terrestrial magnetosphere. Theory and observation suggest that reconnection events are triggered there, leading to particle acceleration. Some of these particles reach the auroral zone, resulting in ionospheric currents that give rise to magnetic field perturbations which are detected at high geomagnetic latitudes by a terrestrial magnetometer chain—the lower trace in figure 11. The expected causal linkage between the two traces thus encompasses multiple

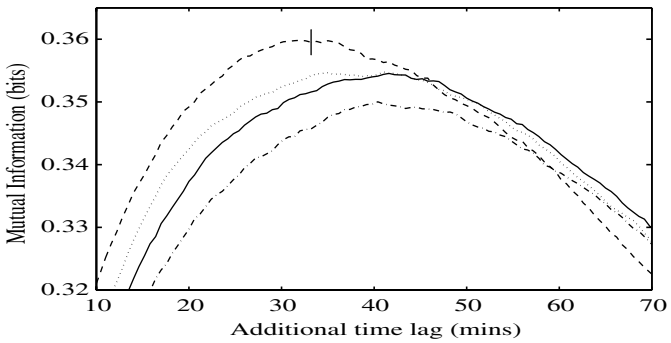

Figure 12. Mutual information content, in bits per bit, shared between the time-shifted upper trace in figure 11 and the lower trace, as a function of the additional time lag $\Delta t'$ [11]. The different curves arise from different solar wind propagation models used to infer Δt from local measurements at the sunward libration point. The error bar of 0.002 bits is shown.

nonlinear plasma phenomena operating over a broad range of lengthscales and timescales. Empirically, this causal linkage is reflected by apparently related gross features and structure in the two traces, with the lower trace time-delayed with respect to the upper in figure 11. Plasma physics issues can be linked to the time delay as follows. First, there is a time delay Δt due to propagation of a given perturbation with the solar wind from the sunward libration point to the outer magnetosphere. A numerical value can be assigned to Δt, based on measurements of solar wind velocity combined with models for solar wind propagation, of which there are several. Second, there is an unknown time delay $\Delta t'$ arising from the multiple plasma phenomena within the magnetosphere that translate the incident perturbation from the magnetospheric boundary down to the terrestrial magnetometer chain.

If the combined plasma system comprising the solar wind and the magnetosphere were a perfect transmitter of information, the lower trace in figure 11 would contain identical information to the upper, indeed it would be a time-shifted version thereof. It is therefore instructive to take the upper trace, time shift it by the sum of the inferred quantity Δt and the free parameter $\Delta t'$, and compute the mutual Shannon information that this time-shifted trace shares with the measured lower trace [11]. Figure 12 plots mutual information content versus the additional time lag $\Delta t'$ as free parameter, for different solar wind propagation models. It yields three items of physical interest. First, mutual information is maximized by the upper dashed line, which is obtained using a Parker spiral model for solar wind propagation. While the difference between the curves corresponding to different models is not great, it exceeds the error bars and could contribute to a more broadly based comparison between solar wind propagation models. Second, mutual information maximizes at 0.360 ± 0.002 bits per bit. This quantifies the causal linkage between the two traces in figure 11. Third, mutual information maximizes when the additional time lag $\Delta t' = 33 \pm 5$ min. This quantifies a physically interesting dynamical timescale, namely the time taken by Earth's magnetosphere to process the incoming information via a sequence of coupled nonlinear multiscale plasma phenomena and transmit it to ground [11].

The information content of these signals can be rendered concrete when viewed from a different perspective, that of the two-dimensional recurrence plot. Recurrence plots are constructed as follows, see [12] and references therein: if a short string of digits beginning at time t_1 in a dataset is identical to that beginning at time t_2, the square at (t_1, t_2) in the recurrence plot is coloured black, otherwise it is left white. This is the simplest form of recurrence plot;

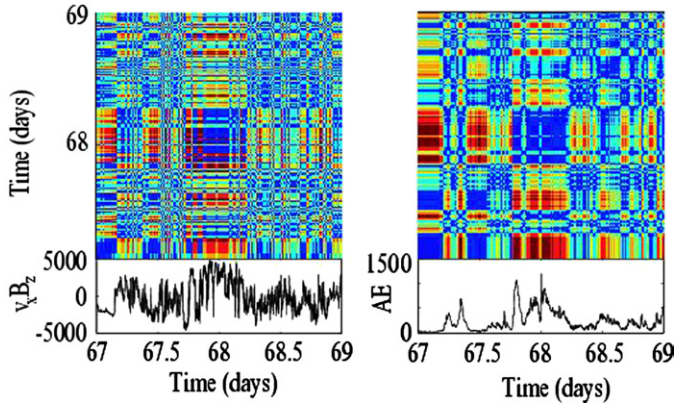

Figure 13. Recurrence plots for space plasma phenomena [11]: solar wind $v_x B_z$ dataset from figure 11, time shifted using the Parker spiral model for Δt, following figure 12 (left); terrestrial magnetometer dataset from figure 11 (right).

subtler versions, such as those shown in figure 13 from [11], quantify the difference between any two strings and represent its magnitude in terms of a colour scale. While there is not space here to describe the mathematical foundations (see, for example [12]), it is intuitively clear that the two signals from figure 11 whose recurrence plots are shown in figure 13 share information insofar as the repeated patterns are the same. Overlaying these two plots, and quantifying their similarity, measures this directly. Indeed, if the colour scale is replaced by a height plotted on the z-axis, so that the recurrence plots become topographical, the volume enclosed between the surface and the plane $z = 0$ maps mathematically to the information content. We refer to [12] for further details of this aspect, including other applications to space plasma physics.

7. Conclusions

We have reviewed a series of pilot studies that apply quantitative techniques, drawn from contemporary complex systems science, to strongly nonlinear datasets obtained from a broad range of fusion, space, solar and astrophysical plasmas. The success of these techniques in capturing and quantifying key aspects of the nonlinear physics could not have been predicted *a priori*. For example, the degree of self-similarity exhibited both by the Cygnus X-1 observations and by the edge turbulence fluctuations in MAST is unexpected and has contributed to the successful application of the growth of range and rescaling techniques described in section 5. As discussed in the introduction, successful models for these plasma systems would need to generate outputs that quantitatively reproduce the features that we have characterized in the real data.

Let us briefly review the physical insights that we have obtained for the different plasmas considered. For the astrophysical x-ray datasets, we have established that the PDFs of the signals from Cygnus X-1 and GRS 1915 + 105 fit extreme value distributions, suggesting that the x-ray detector may pick out the brightest among several concurrent events. These datasets exhibit self-similarity quantified by well-defined Hurst exponents, whose values differ significantly between the different astrophysical sources examined. The differencing and rescaling technique also works well here: this too implies a high degree of self-similarity; it enables the identification of well-defined PDFs for the differenced fluctuations; and it

establishes well-defined timescales over which a single physical process dominates the system behaviour.

These techniques carry over successfully to edge turbulence fluctuations in L-mode and dithering H-mode plasmas in the MAST spherical tokamak, whereas ELMs break up the correlation in full H-mode. We have shown how the new nonlinear techniques, in combination with conventional linear methods, enable a wide ranging quantitative characterization to be constructed. Comparison with the output of numerical models is already under way.

A conceptually simpler question was addressed when we turned to Type III ELMing in selected JET H-mode plasmas. Our aim was to identify—if possible, and this was questionable, given the nonstationarity and sparseness of the data—what class of statistical process drives the observed time series of successive ELM bursts. It can definitely be inferred that one (and only one) of the time series investigated is due to a Poisson process: random, independent and infrequent, a Poisson process differs greatly from the quasiperiodic character usually ascribed to Type III ELMing. It has been suggested that Poisson phenomenology may have arisen because this JET plasma is closer to the H-mode threshold than the other JET plasmas considered. Whether or not this is the case, the statistical study has already thrown additional light on the nature of ELMing and of the H-mode and its threshold. The pursuit of phenomenological correlations and explanations, preferably encompassing many more ELMing plasmas than those considered in this pilot study, is surely desirable. The results reported show that a more rigorous quantitative characterization of ELMing processes is possible, which will complement the existing, more phenomenological, approaches.

In contrast to the study of well-defined ELM bursts, our study of fluctuations in the full-disc solar EUV/XUV irradiance took an integrated global perspective. Instead of defining specific events, and then examining their statistics, we studied fluctuations due to the sum of changes on all lengthscales, irrespective also of their characteristic timescale, across the full system. The fluctuation statistics are found to fit a well-defined power law whose index varies with the solar cycle; we refer to [23], and references therein, for discussion of the possible implications in relation to the basic topological features of multiple-loop magnetic reconnection and the solar magnetic carpet. Here too, the nonideal nature of the plasma data is not an obstacle to systematic statistical analysis—detrending is sufficient to render the data tractable—and the results of the analysis can be used to inform and constrain the physical picture.

The final investigation concerned the causal linkage between strongly nonlinear fluctuations in the upstream solar wind and the corresponding, spatiotemporally separated fluctuations in auroral zone currents. While similar, but time-shifted, features can be identified by the eye in the two time series, here too we have analysed the full time series as they stand, without intervening to first identify ‘events’. The application of Shannon information theory enables us to quantify the mutual information shared between the two sets of measurements. It also provides physical insights: it enables us to distinguish between models for signal propagation in the solar wind; and we are able to quantify the time lag caused by successive plasma processes in the magnetosphere, responding to the incident perturbation by the solar wind and transmitting its consequences down through the magnetosphere to the auroral zone and to Earth. We also noted how recurrence plots can be applied to quantify pattern repetition in strongly nonlinear plasma time series. These initial applications of information theory to plasma nonlinearity and turbulence open the door to more extensive use in this context.

The pilot studies reported in this paper, together with related work (in fusion plasma physics, see for example [31–37] and papers cited therein), represent a significant step forwards in our understanding of strongly nonlinear phenomena in natural and fusion plasmas. Perhaps surprisingly, these complex systems science techniques turn out to work well in this context. They are effective in capturing and quantifying aspects of strongly nonlinear plasma behaviour

that are otherwise difficult to characterize. Furthermore new physical inferences can be drawn from each successful application. While this approach to capturing nonlinearity is novel in plasma physics, it is worth remarking that diverse fields have successfully exploited it, even beyond physics. Two examples will suffice: differencing and rescaling was successfully applied to fluctuations in a leading financial index in 1995 [38]; and the forerunner of recurrence plots, introduced in a physics context in 1987 [39], was developed to quantify repeated patterns of information in genetic nucleotides in 1981 [40].

Rigorous, few-parameter, model-independent characterization of strongly nonlinear plasma datasets is now possible. The numbers that emerge relate directly to the underlying physics and help us to understand it. They also provide a benchmark for comparison of theory with observation; this will enable fair quantitative comparisons between different plasma physics models—in particular, large scale numerical simulations—for a given nonlinear experimental or observational dataset. Similarly, there is now a model-independent basis for characterizing and comparing nonlinear datasets from similar phenomena in different plasma systems. Successful applications already span fusion, space, solar and astrophysical plasmas. We believe that wider adoption of these techniques will be necessary for the development of a more robust predictive capability in this field.

Acknowledgments

It is a pleasure to acknowledge the contributions of many collaborators to the application of complex systems science to plasma physics, including Ben Dudson, Jon Graves, John Greenhough, Per Helander, Bogdan Hnat, Keith Hopcraft, David Hughes, Ken McClements, Thomas March, James Merrifield, Maya Paczuski, George Rowlands and Nick Watkins. This work was supported in part by Euratom and by the United Kingdom Engineering and Physical Sciences Research Council and Particle Physics and Astronomy Research Council.

References

[1] Kantz H and Schreiber T 1997 *Nonlinear Time Series Analysis* (Cambridge: Cambridge University Press)
[2] Badii R and Politi A 1999 *Complexity* (Cambridge: Cambridge University Press)
[3] Sornette D 2000 *Critical Phenomena in Natural Sciences* (Heidelberg: Springer)
[4] Bracewell R N 2000 *The Fourier Transform and its Applications* (Boston: McGraw-Hill)
[5] Tang W M and Chan V S 2005 *Plasma Phys. Control. Fusion* **47** R1
[6] Dudson B D, Dendy R O, Kirk A, Meyer H and Counsell G C 2005 *Plasma Phys. Control. Fusion* **47** 885
[7] Greenhough J, Chapman S C, Dendy R O and Ward D J 2003 *Plasma Phys. Control. Fusion* **45** 747
[8] Greenhough J, Chapman S C, Chaty S, Dendy R O and Rowlands G 2002 *Astron. Astrophys.* **385** 693
[9] Greenhough J, Chapman S C, Chaty S, Dendy R O and Rowlands G 2003 *Mon. Not. R. Astron. Soc.* **340** 851
[10] Greenhough J, Chapman S C, Dendy R O, Nakariakov V and Rowlands G 2003 *Astron. Astrophys.* **409** L17
[11] March T K, Chapman S C and Dendy R O 2005 *Geophys. Res. Lett.* **32** L04101
[12] March T K, Chapman S C and Dendy R O 2005 *Physica* D **200** 171
[13] Bak P, Tang C and Wiesenfeld K 1987 *Phys. Rev. Lett.* **59** 381
[14] Bak P 1996 *How Nature Works* (New York: Copernicus)
[15] Newman D E, Carreras B A, Diamond P H and Hahm T S 1996 *Phys. Plasmas* **3** 1858
[16] Dendy R O and Helander P 1997 *Plasma Phys. Control. Fusion* **39** 1947
[17] Dendy R O and Helander P 1998 *Phys. Rev.* E **57** 3641
[18] Chapman S C 2000 *Phys. Rev.* E **62** 1905
[19] Sanchez R, Newman D E and Carreras B A 2001 *Nucl. Fusion* **41** 247
[20] Chapman S C, Dendy R O and Hnat B 2001 *Phys. Rev. Lett.* **86** 2814
[21] Graves J P, Dendy R O, Hopcraft K I and Jakeman E 2002 *Phys. Plasmas* **9** 1596
[22] Hughes D, Paczuski M, Dendy R O, Helander P and McClements K 2003 *Phys. Rev. Lett.* **90** 131101

[23] Dendy R O, Chapman S C and Paczuski M 2006 *13th Int. Congr. on Plasma Physics (Kiev, Ukraine, 22–26 May 2006) Plasma Phys. Control. Fusion* 2007 **49** at press
[24] Dennis B R 1985 *Solar Phys.* **100** 465
[25] Aschwanden M J *et al* 2000 *Astrophys. J.* **535** 1047
[26] Lu E T and Hamilton R J 1991 *Astrophys. J.* **380** L89
[27] Degeling A W, Martin Y R, Bak P E, Lister J B and Llobet X 2001 *Plasma Phys. Control. Fusion* **43** 1671
[28] Martin Y R, Degeling A W and Lister J B 2002 *Plasma Phys. Control. Fusion* **44** A373
[29] Consolini G 1997 *Cosmic Physics in the Year 2000* (Bologna, Italy: Società Italiana di Fisica) p 123
[30] Shannon C E and Weaver W 1949 *The Mathematical Theory of Communication* (Urbana: University of Illinois Press)
[31] Pedrosa M A *et al* 1999 *Phys. Rev. Lett.* **82** 3621
[32] Beyer P, Sarazin Y, Garbet X, Ghendrih P and Benkadda S 1999 *Plasma Phys. Control. Fusion* **41** A757
[33] Zaslavsky G M *et al* 2000 *Phys. Plasmas* **7** 3691
[34] Antar G Y, Counsell G, Yu Y, Labombard B and Devynck P 2003 *Phys. Plasmas* **10** 419
[35] van Milligen B P, Carreras B A and Sanchez R 2005 *Plasma Phys. Control. Fusion* **47** B743
[36] Garcia O E, Naulin V, Nielsen A H and Juul Rasmussen J 2005 *Phys. Plasmas* **12** 062309
[37] Graves J P, Horacek J, Pitts R A and Hopcraft K I 2005 *Plasma Phys. Control. Fusion* **47** L1
[38] Mantegna R N and Stanley H E 1995 *Nature* **376** 46
[39] Eckmann J-P, Kamphorst S O and Ruelle D 1987 *Europhys. Lett.* **4** 973
[40] Maizel J V and Lenk R P 1981 *Proc. Natl Acad. Sci. USA* **78** 7665